

Article

# Self-Propagating Synthesis and Characterization Studies of Gd-Bearing Hf-Zirconolite Ceramic Waste Forms

Kuibao Zhang <sup>1,3,\*</sup>, Dan Yin <sup>1</sup>, Kai Xu <sup>2</sup> and Haibin Zhang <sup>4,\*</sup>

<sup>1</sup> State Key Laboratory of Environment-friendly Energy Materials, Southwest University of Science and Technology, Mianyang 621010, China; yindan@swust.edu.cn

<sup>2</sup> State Key Laboratory of Silicate Materials for Architectures, Wuhan University of Technology, Wuhan 430070, China; kaixu@whut.edu.cn

<sup>3</sup> Sichuan Civil-Military Integration Institute, Mianyang 621010, China

<sup>4</sup> Institute of Nuclear Physics and Chemistry, China Academy of Engineering Physics, Mianyang 621900, China

\* Correspondence: xiaobao320@163.com (K.Z.); wsschbinzhang@163.com (H.Z.); Tel./Fax: +86-816-241-9492 (K.Z.)

Received: 14 December 2018; Accepted: 30 December 2018; Published: 7 January 2019



**Abstract:** Synroc is recognized as the second-generation waste matrix for nuclear waste disposal. Zirconolite is one of the most durable Synroc minerals. In this study, Gd and Hf were selected as the surrogates of trivalent and tetravalent actinide nuclides. Gd-bearing Hf-zirconolite ( $\text{Ca}_{1-x}\text{Hf}_{1-x}\text{Gd}_{2x}\text{Ti}_2\text{O}_7$ ) ceramic waste forms were rapidly synthesized from a self-propagating technique using CuO as the oxidant. The results indicate that Gd can concurrently replace the Ca and Hf sites. However,  $\text{Gd}_2\text{O}_3$  could not completely be incorporated into the lattice structure of zirconolite when the  $x$  value is higher than 0.8. The aqueous durability of selected Gd-Hf codoped sample (Hf-Gd-0.6) was tested, where the 42 days normalized leaching rates ( $LR_i$ ) of Ca, Cu, Gd and Hf are measured to be 1.57, 0.13,  $4.72 \times 10^{-7}$  and  $1.59 \times 10^{-8} \text{ g}\cdot\text{m}^{-2}\cdot\text{d}^{-1}$ .

**Keywords:** self-propagating; nuclear waste; zirconolite; actinide; aqueous durability

## 1. Introduction

Due to the main contribution of minor actinides (Np, Am, Cm) to the long term radiotoxicity of high-level nuclear wastes (HLW) recovered from spent fuel reprocessing, the separation of the actinide nuclides and their immobilization in durable matrices have been of prime importance [1,2]. A large number of fundamental and engineering orientated studies have been launched in several countries (France, Japan, Russia, et al.) to explore the feasibility of highly stable matrices, such as ceramics, glass-ceramics or glasses [3–15]. Among these host materials, borosilicate glass has been proved as a desirable matrix for large-scale applications [4,11]. However, the low solubility of minor actinides in glass matrix and the relatively low thermal stability of glass are the major limitations for the disposal of actinide-rich wastes [10,16]. Alternatively, Synroc has been proposed as a potential matrix for HLW immobilization by Ringwood et al. [17]. Synroc is mainly composed of multiple titanate mineral phases, such as zirconolite ( $\text{CaZrTi}_2\text{O}_7$ ), pyrochlore ( $\text{A}_2\text{B}_2\text{O}_6\text{X}$ ), perovskite ( $\text{CaTiO}_3$ ), hollandite ( $\text{BaAl}_2\text{Ti}_6\text{O}_{16}$ ), rutile ( $\text{TiO}_2$ ), spinel ( $\text{AB}_2\text{O}_4$ ), et al. These mineral phases have accommodated actinide elements in the natural environment for over tens of millions of years. According to the theory of isomorphism substitution, radioactive nuclides can be included into the lattice structure of above-mentioned mineral phases, which can significantly promote the waste loading and long-term stability [17–23].

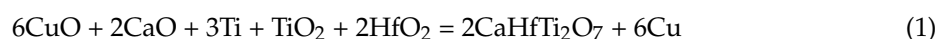
Zirconolite, which is one of the most durable phases among Synroc minerals, has been extensively investigated as a ceramic matrix [24–27]. Zirconolite exhibits a layered structure, which is formed by the stacking layers of edge shared Ti-O polyhedra ( $\text{TiO}_6$  and  $\text{TiO}_5$ ) and layers of  $\text{Ca}^{2+}$  and  $\text{Zr}^{4+}$  ions [25–28]. Due to the composition and nature of substitution, zirconolite can transform into different polytypes like zirconolite-2M (monoclinic), zirconolite-3T (trigonal), zirconolite-3O (orthorhombic). The different forms of coordination make zirconolite structure capable of accommodating large cations like rare-earth, actinide and alkaline earth ions, as well as small cations like transition metal ions [28–30]. Moreover, zirconolite-base waste forms exhibit excellent performances in waste loading, aqueous durability, chemical flexibility, radiation resistance and existence of nature analogues, which make it a potential host phase for the immobilization of separated minor actinides [4,7,8].

In general, zirconolite-rich Synroc waste forms were mainly synthesized by traditional methods, such as liquid phase synthesis (hydroxide and sol-gel methods) and solid state reaction [31–33]. These approaches usually require a long-time sintering process under high-temperature and high pressure, which is time consuming and evokes the risk of nuclide volatilization. Muthuraman et al. have been proposed an alternative synthesis approach, self-propagating high-temperature synthesis (SHS), for the immobilization of nuclear waste [34]. Because of its special advantages [35], SHS technique has been considered as a candidate approach for environment protection, such as stabilization of radioactive and toxic wastes. In recent years, we have explored the rapid synthesis of zirconolite and pyrochlore based waste forms using SHS [36–41]. Quick pressing (QP) was also introduced to obtain highly densified samples. The results demonstrate that highly densified ceramic-based waste forms can be synthesized within several minutes using this SHS/QP technique.

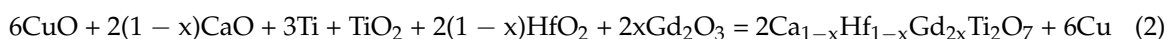
As real actinides contained HLW is not available in laboratory, simulated actinide nuclides are widely employed in fundamental research. From the consideration of crystal chemistry and ionic radius [42], Gd and Ce were usually employed as the surrogates of trivalent and tetravalent actinide elements. From previous studies [43,44], the charge state of Ce is not stable as  $\text{Ce}^{4+}$  usually transforms to  $\text{Ce}^{3+}$  under high temperature sintering. Actually, Hf is a better surrogate of tetravalent actinides (especially Pu) over Ce as the charge state of  $\text{Hf}^{4+}$  is extremely stable. Hf exhibits similar density and solubility as Pu in vitreous waste forms. Hf can also partially or totally replace the Zr site of zirconolite (Hf-zirconolite,  $\text{CaHfTi}_2\text{O}_7$ ) [45,46]. Gd and Hf are considered as a neutron poison for fission reactions because they have extreme high capture cross-sections of thermal neutron [47]. Thus, the Gd-bearing Hf-zirconolite waste forms possess high critical safety when loaded with fissile actinide isotopes of  $^{239}\text{Pu}$  and  $^{235}\text{U}$ . In this study, Hf-zirconolite was rapidly prepared from an SHS/QP technique using CuO as the oxidant. The Zr site was totally replaced by Hf with chemical composition of  $\text{CaHfTi}_2\text{O}_7$ . On this basis,  $\text{Gd}_2\text{O}_3$  was introduced as the surrogate of trivalent actinides, which was designed to concurrently occupy the Ca and Hf sites of Hf-zirconolite. The phase composition, crystal structure, site occupancy and microstructure of the Gd-bearing samples were investigated. In addition, the aqueous durability was evaluated using the standard MCC-1 leaching test [48].

## 2. Materials and Methods

Analytical grade CuO, CaO, Ti,  $\text{TiO}_2$ ,  $\text{ZrO}_2$ , as well as high purity  $\text{Gd}_2\text{O}_3$  and  $\text{HfO}_2$  (purity  $\geq 99.9$  wt. %), were purchased as the raw materials. Firstly, the Hf-zirconolite was prepared according to the following chemical equation:



After that, a series of compositions with stoichiometry as  $\text{Ca}_{1-x}\text{Hf}_{1-x}\text{Gd}_{2x}\text{Ti}_2\text{O}_7$  ( $x = 0.2, 0.4, 0.6, 0.8$  and  $1.0$ ), named as Hf-Gd-0.2, Hf-Gd-0.4, Hf-Gd-0.6, Hf-Gd-0.8 and Hf-Gd-1.0) were synthesized from this SHS technique. The designed SHS reactions were conducted as follows:



The weight percentages of raw materials are listed in Table 1. About 20 g reactants were completely homogenized using planetary ball milling. The mixed powders were then preformed into cylindrical pellets with dimension of  $\Phi 25 \times 12$  mm. The pressed pellets were then ignited and densified similarly to in our previous report [36]. Before pressure exertion, the reaction temperatures of all samples were measured by a W/Re 5/26 thermocouple located at the sample center.

**Table 1.** Weight percentage of the raw reactants for Gd-doped Hf-zirconolite samples.

Sample No.	Addictive Amount of Raw Materials (g)					
	CuO	CaO	HfO <sub>2</sub>	Ti	TiO <sub>2</sub>	Gd <sub>2</sub> O <sub>3</sub>
Hf-Gd-0.2	7.502	1.410	5.294	2.257	1.255	2.279
Hf-Gd-0.4	7.282	1.026	3.854	2.191	1.218	4.426
Hf-Gd-0.6	7.075	0.665	2.496	2.128	1.184	6.450
Hf-Gd-0.8	6.879	0.323	1.213	2.069	1.151	8.362
Hf-Gd-1.0	6.694	-	-	2.014	1.120	10.171

The as-synthesized specimens were pulverized into fine powders, which were characterized by X-ray diffractometer (XRD; D/MAX-RB, Rigaku Corporation, Tokyo, Japan) with Cu K $\alpha$  radiation to obtain the phase composition. The ignited samples were compressed by a quick pressing of 45 MPa with 60 s holding time after about 25–30 s delay of combustion. The obtained samples were then sliced and polished using different grades of emery paper and 0.5  $\mu$ m diamond pastes. After cleaning and drying, the samples were subjected to further characterizations. Microstructure of the selected Hf-Gd-0.6 sample was typically observed using field-emission scanning electron microscopy (FESEM; Zeiss Ultra-55, Oberkochen, Germany) under 15 KV energy. The phase composition and elemental distribution were analyzed from the results of energy-dispersive X-ray spectrometer (EDX, ULTRA 55, ZEISS, Oberkochen, Germany) attached with the FESEM equipment. The chemical durability of Hf-Gd-0.6 sample was evaluated using standard MCC-1 leaching test. The specimen was sliced and grinded into dimension of 5.28 mm  $\times$  5.30 mm  $\times$  5.24 mm, which was suspended by a copper wire and immersed in 80 mL deionized water. Completely cleaned polytetra-fluoroethylene (PTFE) was utilized the leaching container. The leaching tests were carried out at 90 °C with durations of 1, 3, 7, 14, 21, 28, 35 and 42 days. The elemental concentrations of Ca and Cu in the leachates were obtained by inductively coupled plasma (ICP) analysis (iCPA 6500, ThermoFisher, Waltham, MA, USA), while Hf and Gd were collected by inductively coupled plasma-mass spectrometry (ICP-MS) analysis using an Agilent 7700 $\times$  spectrometer (Santa Clara, CA, USA).

### 3. Results and Discussion

#### 3.1. Combustion Temperature and XRD Analysis of the Hf-Zirconolite Sample

According to the previous research [45], Hf can totally replace the Zr site of zirconolite. In this experiment, we firstly testify the feasibility for the SHS preparation of Hf-zirconolite. The combustion experiment of the above-mentioned Equation (1) was conducted. The result demonstrates that the green body can be successfully ignited with self-sustaining reaction. The combustion lasts for about 10 s after ignition, which leads to a reaction speed of about 2–3 mm/s. The center temperature of this sample was measured as depicted in Figure 1a. The maximum temperature is 1177 °C and the temperature duration ( $\geq 1000$  °C) is longer than 30 s. As there is heat dissipation during the combustion reaction and subsequent testing, the real temperature should be much higher than the measured one. This temperature is adequate and beneficial for subsequent compression as it is higher than the melting point of Cu (1083 °C). Figure 1b shows the XRD pattern of the obtained Hf-zirconolite sample, which indicates the phase composition mostly conforms to the original design. Hf-zirconolite and Cu demonstrate are the main phases with a trace of CaTiO<sub>3</sub> phase. As no peaks correspond to HfO<sub>2</sub>, we can confirm that HfO<sub>2</sub> has been completely incorporated into the Zr site of zirconolite.

Because the  $Zr^{4+}$  and  $Hf^{4+}$  cations are in the same charge state and close ionic radius (0.72 Å for  $Zr^{4+}$  and 0.71 Å for  $Hf^{4+}$ ), they can mutually substituted under random proportion. This result testifies that Hf-zirconolite can be readily synthesized using the SHS method.

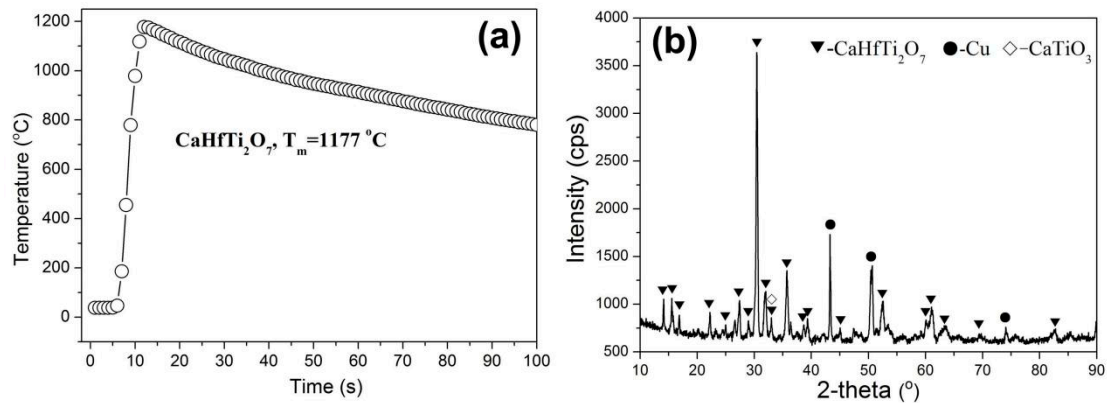


**Figure 1.** (a) Reaction temperature of the Hf-zirconolite sample, (b) XRD pattern of the Hf-zirconolite sample.

### 3.2. Reaction Temperature and Phase Composition of Gd-Bearing Hf-Zirconolite Samples

The Gd-bearing Hf-zirconolite waste forms were subsequently synthesized. All the designed SHS reactions were successfully ignited and the combustions lasted for about 10 s after tungsten wire ignition. The center temperatures were collected and depicted in Figure 2a. There is not a trend of regularity for the temperature of Gd-bearing samples. The maximum temperatures of these five samples reach to 1392 °C, 1120 °C, 1403 °C, 1458 °C and 1298 °C as the x value is elevated from 0.2 to 1.0. Compared with the original Hf-zirconolite (1177 °C), the Gd<sub>2</sub>O<sub>3</sub> doped samples exhibit much higher temperatures (except for the Hf-Gd-0.4 sample). This result reveals that the reactivity of Gd<sub>2</sub>O<sub>3</sub> is higher than CaO or/and HfO<sub>2</sub>. Although the temperatures are not high, they are adequate and facilitate the subsequent densification process to get highly densified samples.

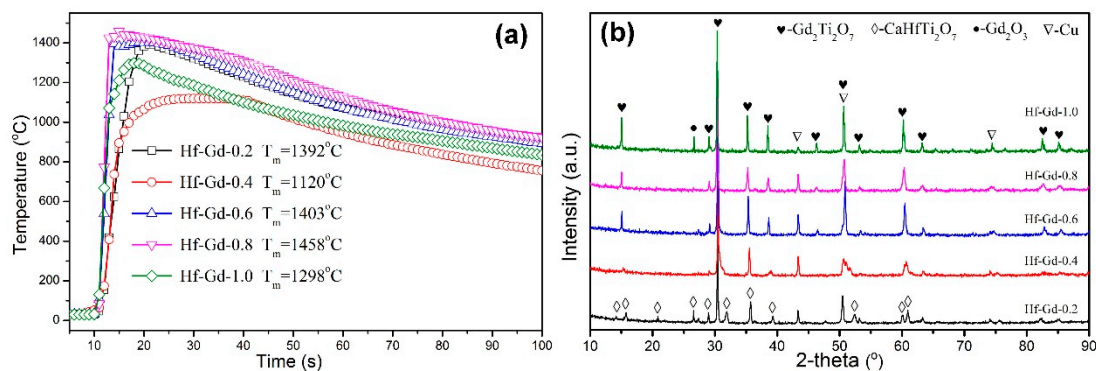


**Figure 2.** (a) Reaction temperatures, (b) XRD patterns of the Gd-bearing Hf-zirconolite samples with x values of 0.2–1.0.

According to previous studies [29,31], the Ca and Zr site of zirconolite could be concurrently occupied by trivalent actinides. The phase compositions of Gd-bearing Hf-zirconolite samples were characterized with the XRD patterns presented in Figure 2b. It is distinctly demonstrated that there is a phase transformation from 2M-zirconolite to cubic pyrochlore as the x value is elevated. There are only Hf-zirconolite (CaHfTi<sub>2</sub>O<sub>7</sub>, PDF No. 84-0163) and Cu phases in the Hf-Gd-0.2 sample. Minor pyrochlore appears when the x value is 0.4. The pyrochlore phase demonstrates as the main phase when the x value is 0.6, which can be verified by the superlattice (100) diffraction peak at around 15°. This result is similar as the Nd-bearing zirconolite in the solid-state synthesized

CaZrTi<sub>2</sub>O<sub>7</sub>-Nd<sub>2</sub>Ti<sub>2</sub>O<sub>7</sub> system [31]. However, unreacted Gd<sub>2</sub>O<sub>3</sub> is detected in the Hf-Gd-1.0 sample, which indicates that Gd could not totally substitute the Ca and Hf sites. This phenomenon may be related with the highly different ionic radius between Gd<sup>3+</sup> (0.938 Å) and Hf<sup>4+</sup> (0.71 Å). The maximum loading capacity of Gd<sub>2</sub>O<sub>3</sub> is the Hf-Gd-0.8 sample, and only Gd<sub>2</sub>Ti<sub>2</sub>O<sub>7</sub>-based pyrochlore (PDF No. 73-1698) and Cu are demonstrated as the constituent phases in this sample.

### 3.3. SEM and EDX Analysis of the Gd-Doped Samples

The observed phase fields in the Ca<sub>1-x</sub>Hf<sub>1-x</sub>Gd<sub>2x</sub>Ti<sub>2</sub>O<sub>7</sub> system were further supported by the SEM and EDX analysis. Typical back-scattered electron (BSE) image of the selected Hf-Gd-0.6 sample is shown in Figure 3a. No obvious pores can be observed in the surface image, which indicates this sample was well densified. Meanwhile, two different phases with distinct contrasts can be detected in the polish surface. The ceramic matrix phase is labeled as “A” and the metallic Cu phase is labelled as “B”. The Cu phase can be readily determined because it is segregated by a distinct boundary. The brightness of “A” district is obviously higher than “B”, which is attributed to the higher atomic number over Cu for Ca<sub>1-x</sub>Hf<sub>1-x</sub>Gd<sub>2x</sub>Ti<sub>2</sub>O<sub>7</sub> phase. According to the XRD result, the ceramic matrix should be pyrochlore-based titanate with a small amount of zirconolite phase. Figure 3b presents the fracture surface of Hf-Gd-0.6 sample, which exhibits a dense microstructure with tightly contacted submicron sized grains. The grain boundary is not very clear in the polishing surface and fracture surface, which reveals the feature of combustion synthesis as the reaction speed is high and soaking time is short. There is no time for the formation of grain boundary and grain growth.

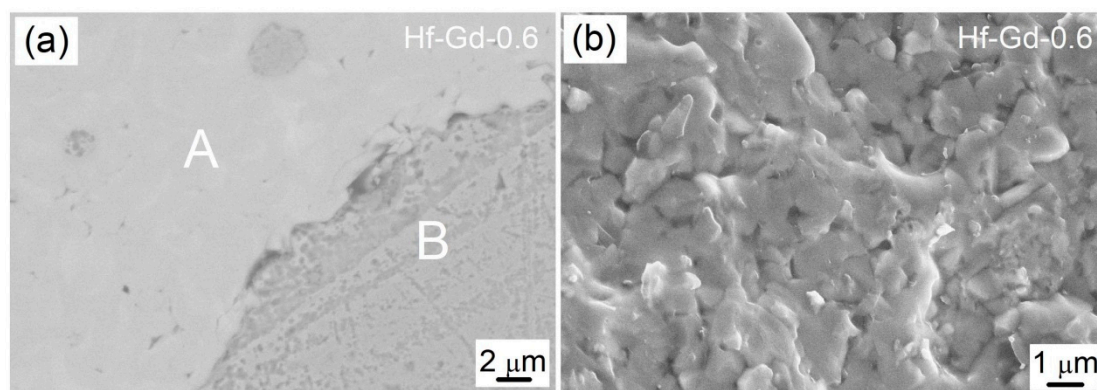


**Figure 3.** SEM images of the Hf-Gd-0.6 sample: (a) the polished surface, (b) the fracture surface.

Elemental EDX characterization was further conducted to determine the phase composition and elemental distribution of the typical Hf-Gd-0.6 specimen. The BSE and EDX mapping images are presented in Figure 4, where all the metallic elements of Ca, Ti, Hf, Gd and Cu are listed. The representative BSE image of Figure 4a supports the coexistence of “A” and “B” phases. Obviously, the “B” area must be Cu phase, which is testified by the EDX mapping image of Figure 4d. The “A” phase should be Ca<sub>1-x</sub>Hf<sub>1-x</sub>Gd<sub>2x</sub>Ti<sub>2</sub>O<sub>7</sub> phase as the Ca, Ti, Gd elements are enriched in this area. This result conforms to the phase composition of XRD analysis. It’s worth noting that Hf not only appears in the matrix A area but also in the Cu phase. The enrichment of Cu and Hf elements is slightly overlapping in the “B” area. This phenomenon is strange as there is no peak corresponding to Hf or HfO<sub>2</sub> in the XRD pattern. It may be attributed to the adjacent energy characteristic peaks of Cu and Hf in the EDX spectra (Hf: K<sub>α</sub> = 8.040, K<sub>β</sub> = 8.903, Cu: K<sub>α</sub> = 7.898, K<sub>β</sub> = 9.021).

The EDX spotting analysis was further conducted to determine the chemical composition of the constituent ceramic phase, where the results are demonstrated in Figure 5. The EDX spotting analysis demonstrates that Hf has not been detected in the Cu phase. The EDX spotting image of “A” phase in Figure 5a is presented in Figure 5b. Similar as the EDX mapping results, the existence of Ca, Ti, Zr, Hf and O in the EDX spotting spectra indicates that the “A” phase is Gd and Hf doped

pyrochlore phase. At least five points of “A” area were calculated to obtain the average elemental quantities as listed in Figure 5b. Based on this data, the chemical formulation of ceramic phase is calculated as  $\text{Ca}_{0.39}\text{Hf}_{0.37}\text{Gd}_{1.38}\text{Ti}_{1.80}\text{O}_7$ . Compared with the designed formulation of Hf-Gd-0.6 sample ( $\text{Ca}_{0.4}\text{Hf}_{0.4}\text{Gd}_{1.2}\text{Ti}_2\text{O}_7$ ), the obtained ceramic phase is slightly deficient in Ti while rich in Gd. The Ca and Hf elements are very close to the designed values. This result testifies that the ceramic phase is in pyrochlore structure, where the Ca and Hf elements occupy the A site (Gd site in this study) of  $\text{A}_2\text{B}_2\text{O}_7$  pyrochlore.

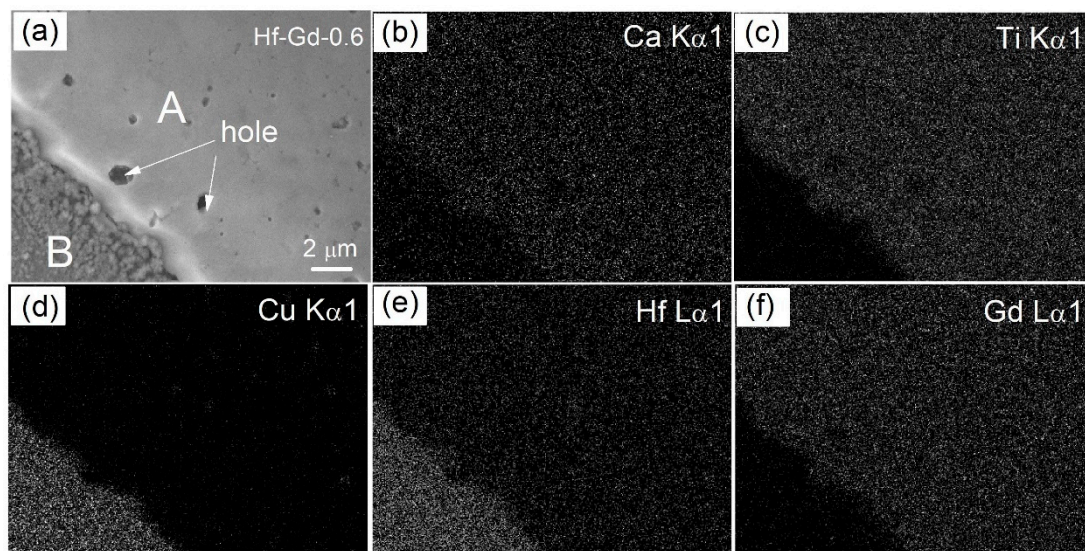


**Figure 4.** SEM-EDX mapping images of the Hf-Gd-0.6 sample: (a) representative BSE image, (b–f) elemental distribution of Ca, Ti, Cu, Hf and Gd elements.

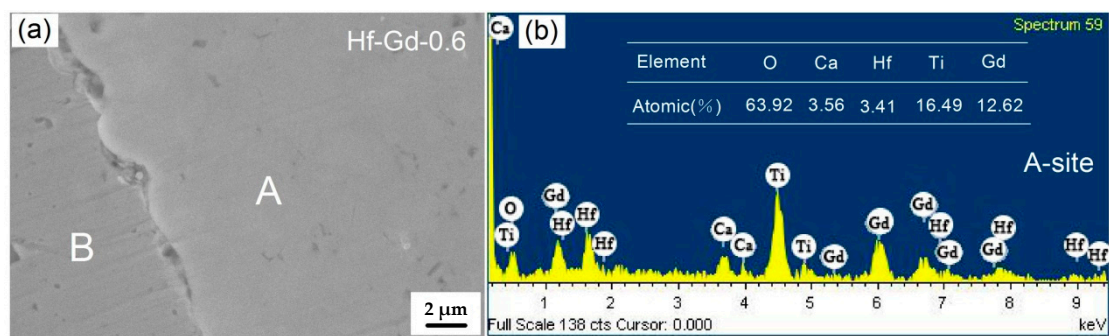


**Figure 5.** EDX spotting results of the Hf-Gd-0.6 sample: (a) representative BSE image, (b) elemental spotting analysis of the “A” region.

### 3.4. Chemical Stability of the Hf-Gd-0.6 Sample

The representative Hf-Gd-0.6 specimen was selected for the standard MCC-1 leaching test. The 1–42 days normalized elemental leaching rate of Ca, Cu, Gd and Hf are computed and depicted in Figure 6a–d. With the increase of soaking duration, all the normalized leaching rates firstly decrease in 1–7 days. However, the  $LR_{\text{Cu}}$  and  $LR_{\text{Gd}}$  exhibit slight ascension when the leaching time is prolonged (7 days for Cu and 21 days for Gd). Anyhow, the  $LR_{\text{Ca}}$  and  $LR_{\text{Cu}}$  values are  $1.57 \text{ g}\cdot\text{m}^{-2}\cdot\text{d}^{-1}$  and  $0.13 \text{ g}\cdot\text{m}^{-2}\cdot\text{d}^{-1}$  after 42 days. Gd and Hf are highly durable elements as shown in Figure 6c,d. Although there is a slight increase, the 42 days  $LR_{\text{Gd}}$  value is as low as  $4.72 \times 10^{-7} \text{ g}\cdot\text{m}^{-2}\cdot\text{d}^{-1}$ . The  $LR_{\text{Hf}}$  value exhibits a congruent decrease tendency during 1–42 days leaching, where the leaching rate is  $1.11 \times 10^{-8} \text{ g}\cdot\text{m}^{-2}\cdot\text{d}^{-1}$  after 42 days. In this experiment, the leaching rate of Ca and Cu is comparable while Gd and Hf are even lower than Synroc waste forms prepared by hot pressing (HP)

or hot isostatic pressing (HIP) [32,33]. The leaching rates are also significantly lower than borosilicate glass (about  $1 \text{ g}\cdot\text{m}^{-2}\cdot\text{d}^{-1}$ ,  $90 \text{ }^\circ\text{C}$ ) [2,3,49].

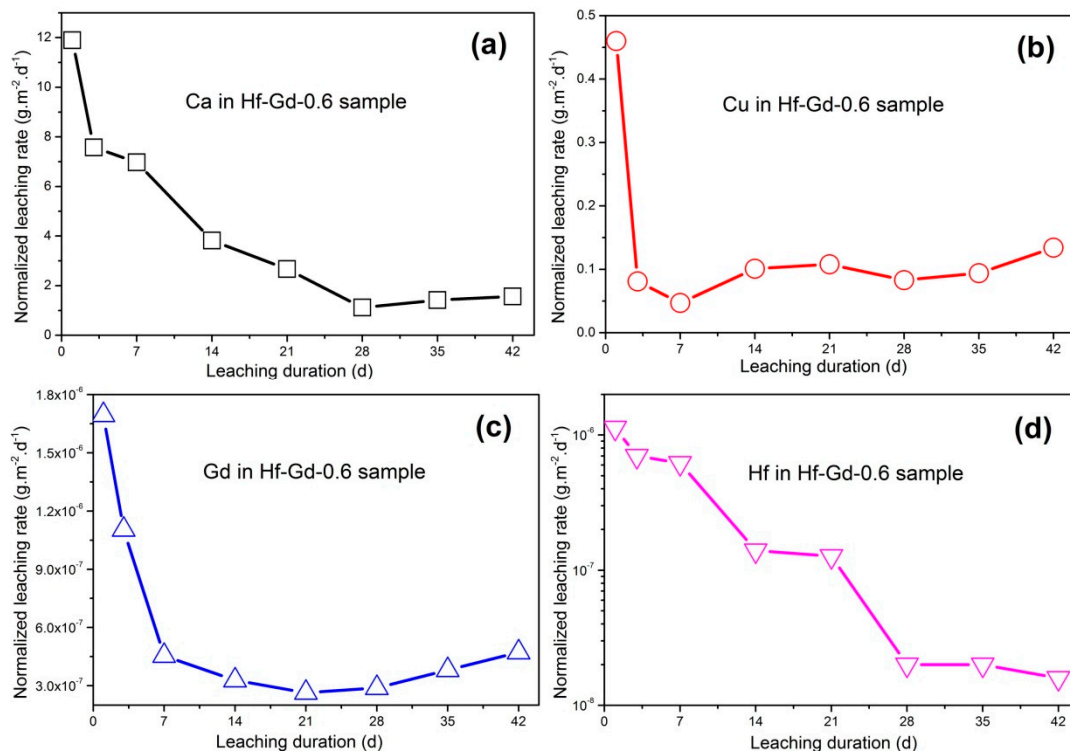


**Figure 6.** 1–42 days normalized leaching rates of the Hf-Gd-0.6 sample: (a) element Ca, (b) element Cu, (c) element Gd, (d) element Hf.

#### 4. Conclusions

In this study, Gd-bearing Hf-zirconolite ( $\text{Ca}_{1-x}\text{Hf}_{1-x}\text{Gd}_{2x}\text{Ti}_2\text{O}_7$ ) waste forms were rapidly synthesized from the SHS/QP method using CuO as the oxidant. Gd and Hf were employed as the simulants of trivalent and tetravalent actinides. The results indicate that Hf can totally replace the Zr site using this SHS process, and Gd can concurrently replace the Ca and Hf sites (Gd preferentially substitutes the Ca site).  $\text{Gd}_2\text{O}_3$  could not completely be incorporated into the lattice structure of zirconolite when the  $x$  value is higher than 0.8. The aqueous durability of selected Hf-Gd-0.6 sample was tested, where the 42 days normalized leaching rates ( $LR_i$ ) of Ca, Cu, Gd and Hf are measured to be  $1.57$ ,  $0.13$ ,  $4.72 \times 10^{-7}$  and  $1.59 \times 10^{-8} \text{ g}\cdot\text{m}^{-2}\cdot\text{d}^{-1}$ . These results demonstrate that the SHS/QP route is suitable for the preparation of zirconolite and pyrochlore based waste forms for HLW immobilization.

**Author Contributions:** Conceptualization, K.Z. and H.Z.; Methodology, K.Z. and D.Y.; Formal Analysis, D.Y. and K.X.; Writing—Original Draft Preparation, D.Y.; Writing—Review & Editing, K.Z.

**Funding:** This research was funded by the National Natural Science Foundation of China (No. 51202203, 51672228), the Project of State Key Laboratory of Environment-friendly Energy Materials (Southwest University of Science and Technology, No. 16kffk05, 17FKSY0104) and Science Development Foundation of China Academy of Engineering Physics.

**Conflicts of Interest:** The authors declare no conflicts of interest.

#### References

- International Atomic Energy Agency. *Design and Operation of High Level Waste, Vitrification and Storage Facility*; Technical Report Series No. 176; IAEA: Vienna, Austria, 1977.
- Ojovan, M.I.; Lee, W.E. *An Introduction to Nuclear Waste Immobilization*; Elsevier Ltd.: Oxford, UK, 2005; pp. 213–267.

3. Caurant, D.; Loiseau, P.; Majérus, O.; Aubin-Chevaldonnet, V.; Bardez, I.; Quintas, A. *Glass, Glass-Ceramics and Ceramics for Immobilization of Highly Radioactive Nuclear Wastes*; Nova Science Publishers: New York, NY, USA, 2009.
4. Ewing, R.C. Nuclear waste forms for actinides. *Proc. Natl. Acad. Sci. USA* **1999**, *96*, 3432–3439. [[CrossRef](#)] [[PubMed](#)]
5. Lee, W.E.; Ojovan, M.I.; Stennett, M.C.; Hyatt, N.C. Immobilisation of radioactive waste in glasses, glass composite materials and ceramics. *Adv. Appl. Ceram.* **2006**, *105*, 3–12. [[CrossRef](#)]
6. Donald, I.W.; Metcalfe, B.L.; Taylor, R.N.J. The immobilization of high level radioactive wastes using ceramics and glasses. *J. Mater. Sci.* **1997**, *32*, 5851–5887. [[CrossRef](#)]
7. Vance, E.R.; Lumpkin, G.R.; Carter, M.L.; Cassidy, D.J.; Ball, C.J.; Day, R.A.; Begg, B.D. Incorporation of uranium in zirconolite (CaZrTi<sub>2</sub>O<sub>7</sub>). *J. Am. Ceram. Soc.* **2002**, *85*, 1853–1859. [[CrossRef](#)]
8. Ewing, R.C.; Weber, W.J.; Lian, J. Nuclear waste disposal-pyrochlore A<sub>2</sub>B<sub>2</sub>O<sub>7</sub>: Nuclear waste form for the immobilization of plutonium and “minor” actinides. *J. Appl. Phys.* **2004**, *95*, 5929–5971. [[CrossRef](#)]
9. Loiseau, P.; Caurant, D.; Baffier, N.; Mazerolles, L.; Fillet, C. Glass-ceramic nuclear waste forms obtained from SiO<sub>2</sub>-Al<sub>2</sub>O<sub>3</sub>-CaO-ZrO<sub>2</sub>-TiO<sub>2</sub> glasses containing lanthanides (Ce, Nd, Eu, Gd, Yb) and actinides (Th): Study of internal crystallization. *J. Nucl. Mater.* **2004**, *335*, 827–837. [[CrossRef](#)]
10. Caurant, D.; Majérus, O.; Losieau, P.; Bardez, I.; Baffier, N.; Dussossoy, J.L. Crystallization of neodymium-rich phases in silicate glasses developed for nuclear waste immobilization. *J. Nucl. Mater.* **2006**, *354*, 143–162. [[CrossRef](#)]
11. Weber, W.J.; Navrotsky, A.; Stefanovsky, S.; Vance, E.R.; Vernaz, E. Materials science of high-level nuclear waste immobilization. *MRS Bull.* **2009**, *34*, 46–53. [[CrossRef](#)]
12. Vance, E.R. Synroc: A suitable waste form for actinides. *MRS Bull.* **1994**, *19*, 28–32. [[CrossRef](#)]
13. Ojovan, M.I.; Lee, W.E. *New Developments in Glassy Nuclear Wasteforms*; Nova Science Publishers: New York, NY, USA, 2007.
14. Donald, I.W. *Waste Immobilization in Glass and Ceramic Based Hosts. Radioactive, Toxic and Hazardous Waste*; Wiley: Chichester, UK, 2010.
15. Stefanovsky, S.V.; Yudinsev, S.V.; Gieré, R.; Lumpkin, G.R. Nuclear waste forms. In *Energy, Waste and the Environment: A Geochemical Perspective*; Special Publications; Gieré, R., Stille, P., Eds.; Geochemical Society: London, UK, 2004; Volume 236, pp. 37–63.
16. Loiseau, P.; Caurant, D.; Majerus, O.; Baffier, N.; Fillet, C. Crystallization study of (TiO<sub>2</sub>, ZrO<sub>2</sub>)-rich SiO<sub>2</sub>-Al<sub>2</sub>O<sub>3</sub>-CaO glasses. Part II. Surface and internal crystallization processes investigated by differential thermal analysis (DTA). *J. Mater. Sci.* **2003**, *38*, 843–852. [[CrossRef](#)]
17. Ringwood, A.E.; Kesson, S.E.; Ware, N.G.; Hibberson, W. Immobilization of high level nuclear reactor wastes in SYNROC. *Nature* **1979**, *278*, 219–223. [[CrossRef](#)]
18. Vance, E.R.; Ball, C.J.; Day, R.A.; Smith, K.L.; Blackford, M.G.; Begg, B.D.; Angel, P.J. Actinide and rare earth incorporation into zirconolite. *J. Alloy. Compd.* **1994**, *213–214*, 406–409. [[CrossRef](#)]
19. Begg, B.D.; Vance, E.R.; Conradson, S.D. The incorporation of plutonium and neptunium in zirconolite and perovskite. *J. Alloy. Compd.* **1998**, *271–273*, 221–226. [[CrossRef](#)]
20. Peng, L.; Zhang, K.B.; Yin, D.; Wu, J.J. Self-propagating synthesis, mechanical property and aqueous durability of Gd<sub>2</sub>Ti<sub>2</sub>O<sub>7</sub> pyrochlore. *Ceram. Int.* **2016**, *42*, 18907–18913. [[CrossRef](#)]
21. Zhang, K.B.; He, Z.S.; Peng, L.; Zhang, H.; Lu, X. Self-propagating synthesis of Y<sub>2–x</sub>Nd<sub>x</sub>Ti<sub>2</sub>O<sub>7</sub> pyrochlore and its aqueous durability as nuclear waste form. *Scr. Mater.* **2018**, *146*, 300–303. [[CrossRef](#)]
22. He, Z.S.; Zhang, K.B.; Yin, D.; Peng, L.; Zhao, W.W. Self-propagating plus quick pressing synthesis and characterizations of Gd<sub>2–x</sub>Nd<sub>x</sub>Ti<sub>1.3</sub>Zr<sub>0.7</sub>O<sub>7</sub> (0 ≤ x ≤ 1.4) pyrochlores. *J. Nucl. Mater.* **2018**, *504*, 61–67. [[CrossRef](#)]
23. Zhang, K.B.; Wen, G.J.; Zhang, H.B.; Teng, Y.C. Self-Propagating high-temperature synthesis of Y<sub>2</sub>Ti<sub>2</sub>O<sub>7</sub> pyrochlore and its aqueous durability. *J. Nucl. Mater.* **2015**, *465*, 1–5. [[CrossRef](#)]
24. Rossell, H.J. Zirconolite—A fluorite-related superstructure. *Nature* **1980**, *283*, 282–283. [[CrossRef](#)]
25. Gatehouse, B.M.; Grey, I.E.; Hill, R.J.; Rossell, H.J. Zirconolite, CaZr<sub>x</sub>Ti<sub>3–x</sub>O<sub>7</sub>; structure refinement for near-end-member composition with x = 0.85 and 1.30. *Acta Cryst. B* **1981**, *37*, 306–312. [[CrossRef](#)]
26. Rossell, H.J. Solid solution of metal oxides in the zirconolite phase CaZrTi<sub>2</sub>O<sub>7</sub>. I. Heterotype solid solution. *J. Solid State Chem.* **1992**, *99*, 38–51. [[CrossRef](#)]
27. Cheray, R.W. Zirconolite CaZr<sub>0.92</sub>Ti<sub>2.08</sub>O<sub>7</sub> at 295 K to 1173 K. *J. Solid State Chem.* **1992**, *98*, 323–329. [[CrossRef](#)]

28. White, T.J. The microstructure and microchemistry of synthetic zirconolite, zirkelite and related phases. *Am. Mineral.* **1984**, *69*, 1156–1172.
29. Coelho, A.; Cheary, R.W.; Smith, K.L. Analisis and structural determination of Nd-substituted zirconolite-4M. *J. Solid State Chem.* **1997**, *129*, 346–359. [[CrossRef](#)]
30. Subramanian, M.A.; Aravamudan, G.; Subbba Rao, G.V. Oxide pyrochlores—A review. *Prog. Solid State Chem.* **1983**, *15*, 55–143. [[CrossRef](#)]
31. Jafar, M.; Sengupta, P.; Achary, S.N.; Tyagi, A.K. Phase evolution and microstructural studies in CaZrTi<sub>2</sub>O<sub>7</sub>-Nd<sub>2</sub>Ti<sub>2</sub>O<sub>7</sub> system. *J. Am. Ceram. Soc.* **2014**, *97*, 609–616. [[CrossRef](#)]
32. Teng, Y.C.; Wang, S.L.; Huang, Y.; Zhang, K.B. Low-temperature reaction hot-pressing of cerium-doped titanate composite ceramics and their aqueous stability. *J. Eur. Ceram. Soc.* **2014**, *34*, 985–990. [[CrossRef](#)]
33. Zhang, Y.; Stewart, M.W.A.; Li, H.; Carter, M.I.; Vance, E.R.; Moricca, S. Zirconolite-rich titanate ceramics for immobilization of actinides-Waste form/HIP can interaction and chemical durability. *J. Nucl. Mater.* **2009**, *395*, 67–74. [[CrossRef](#)]
34. Muthuraman, M.; Patil, K.C.; Senbagaraman, S.; Umarji, A.M. Sintering, microstructure and dilatometric studies of combustion synthesized Synroc phases. *Mater. Res. Bull.* **1996**, *32*, 1375–1381. [[CrossRef](#)]
35. Glagovskii, É.M.; Kuprin, A.V.; Pelevin, L.P.; Kononov, E.E.; Starkov, O.V.; Levakov, E.V.; Postnikov, A.Y.; Lisitsa, F.D. Immobilization of high-level wastes in stable mineral-like materials in a self-propagating high-temperature synthesis regime. *Atom. Energy* **1999**, *87*, 514–518. [[CrossRef](#)]
36. Zhang, K.B.; Wen, G.J.; Yin, D.; Zhang, H.B. Self-propagating high-temperature synthesis of Ce-bearing zirconolite-rich minerals using Ca(NO<sub>3</sub>)<sub>2</sub> as the oxidant. *J. Nucl. Mater.* **2015**, *467*, 214–223. [[CrossRef](#)]
37. Zhang, K.B.; Wen, G.J.; Zhang, H.B.; Teng, Y.C. Self-propagating high-temperature synthesis of CeO<sub>2</sub> incorporated zirconolite-rich waste forms and the aqueous durability. *J. Eur. Ceram. Soc.* **2015**, *35*, 3085–3093. [[CrossRef](#)]
38. He, Z.S.; Zhang, K.B.; Xue, J.L.; Zhao, W.W.; Zhang, H.B. Self-propagating chemical furnace synthesis of nanograin Gd<sub>2</sub>Zr<sub>2</sub>O<sub>7</sub> ceramic and its aqueous durability. *J. Nucl. Mater.* **2018**, *512*, 385–390. [[CrossRef](#)]
39. Peng, L.; Zhang, K.B.; He, Z.S.; Yin, D.; Xue, J.; Xu, C.; Zhang, H. Self-propagating high-temperature synthesis of ZrO<sub>2</sub> incorporated Gd<sub>2</sub>Ti<sub>2</sub>O<sub>7</sub> pyrochlore. *J. Adv. Ceram.* **2018**, *7*, 41–49. [[CrossRef](#)]
40. Zhang, K.B.; He, Z.S.; Xue, J.L.; Zhao, W.W.; Zhang, H.B. Self-propagating synthesis of Y<sub>2-x</sub>Nd<sub>x</sub>Ti<sub>2</sub>O<sub>7</sub> pyrochlores using CuO as the oxidant and its characterizations as waste form. *J. Nucl. Mater.* **2018**, *507*, 93–100. [[CrossRef](#)]
41. Zhang, K.B.; Yin, D.; Han, P.W.; Zhang, H.B. Two-step synthesis of zirconolite-rich ceramic waste matrix and its physicochemical properties. *Int. J. Appl. Ceram. Technol.* **2018**, *15*, 171–178. [[CrossRef](#)]
42. Seaburg, G.T. Overview of actinide and lanthanide (the f) elements. *Radiochim. Acta* **1993**, *61*, 115–122. [[CrossRef](#)]
43. Holgado, J.P.; Alvarez, R.; Munuera, G. Study of CeO<sub>2</sub> XPS spectra by factor analysis: Reduction of CeO<sub>2</sub>. *Appl. Surf. Sci.* **2000**, *161*, 301–315. [[CrossRef](#)]
44. Zhang, K.B.; Yin, D.; Peng, L.; Wu, J.J. Self-propagating synthesis and CeO<sub>2</sub> immobilization of zirconolite-rich composites using CuO as the oxidant. *Ceram. Int.* **2017**, *43*, 1415–1423. [[CrossRef](#)]
45. Caurant, D.; Loiseau, P.; Bardez, I. Structural characterization of Nd-doped Hf-zirconolite Ca<sub>1-x</sub>Nd<sub>x</sub>HfTi<sub>2-x</sub>Al<sub>x</sub>O<sub>7</sub> ceramics. *J. Nucl. Mater.* **2017**, *407*, 88–99. [[CrossRef](#)]
46. Perera, D.S.; Stewart, M.W.A.; Li, H.; Day, R.A.; Vance, E.R. Tentative Phase Relationships in the System CaHfTi<sub>2</sub>O<sub>7</sub>-Gd<sub>2</sub>Ti<sub>2</sub>O<sub>7</sub> with up to 15 mol% Additions of Al<sub>2</sub>TiO<sub>5</sub> and MgTi<sub>2</sub>O<sub>5</sub>. *J. Am. Ceram. Soc.* **2002**, *85*, 2919–2924. [[CrossRef](#)]
47. Emsley, J. *The Elements*; Clarendon Press: Oxford, UK, 1992.
48. ASTM C1220-98. *Standard Test Method for Static Leaching of Monolithic Wasteforms for Disposal of Radioactive Waste*; ASTM International: West Conshohocken, PA, USA, 1998.
49. Smith, K.L.; Lumpkin, G.R.; Blackford, M.G.; Day, R.A.; Hart, K.P. The durability of Synroc. *J. Nucl. Mater.* **1992**, *190*, 287–294. [[CrossRef](#)]

